Ventral-to-dorsal electrocyte development in electric organs of electric eel (*Electrophorus*).

Sinlapachai Senarat [1, 2], Ayako Matsumoto [3], Shintaro Sakaki [2], Daichi Tsuzuki [2], Kazuko Uchida [4], Makoto Kuwahara [4], Eiichi Hondo [2, 3] and Atsuo Iida [2, 3, *]

[1] Division of Biological Science, Faculty of Science, Prince of Songkla University, Kho Hong, Hat Yai District, Songkhla 90110, Thailand

[2] Department of Animal Sciences, Graduate School of Bioagricultural Sciences, Nagoya University, Furo-cho, Chikusa-ku, Nagoya, 464-8601, Japan

[3] Department of Animal Sciences, School of Agriculture, Nagoya University, Furo-cho, Chikusa-ku, Nagoya, 464-8601, Japan

[4] Institute of Materials and Systems for Sustainability, Nagoya University, Furo-cho, Chikusa-ku, Nagoya, 464-8601, Japan

***Correspondence:** Atsuo Iida

Email: tol2.4682@gmail.com

Keywords: cell differentiation, electrocytes, Electrophorus, Na^+/K^+-ATPase

Abstract

Electric eels (*Electrophorus*) are renowned for their ability to generate electric discharge, which is used for prey capture and defense. Their electric organs (EOs) are located along the lateral–ventral region of the tail and contain electrocytes, which are multinucleated syncytium cells. Two major hypotheses for the electrocyte origin are proposed: (1) muscle fibers or their precursors, and (2) mesodermal cells not via muscle lineage. In this study, we demonstrate the likely molecular mechanisms and processes involved in this differentiation, supporting the second hypothesis. We report the regional differences in cell morphology within the main EO (mEO) of *Electrophorus*. The cell morphology and distribution from the ventral terminal to the dorsal region of the mEO suggest the segregation of progenitors from the ventral cluster and their gradual transformation into mature multinucleated electrocytes via the layering and proliferation stages along the dorsal axis. Myosin-positive muscle cells were not included in the mEO differentiation process. Immunohistochemistry revealed strong expression of sodium-potassium adenosine triphosphatase (Na^+/K^+-ATPase), a key component in generating electric discharge in the mEO, across most mEO regions, except in the ventral cluster cells. Based on these observations, we propose that electrocyte progenitors develop from ventral cluster cells in the mEO and differentiate into mature multinucleated cells as they migrate dorsally. This is the first report to approach the developmental process of *Electrophorus* electrocytes from cell morphology and genetic profiles. Our findings represent a breakthrough in understanding the differentiation of electrocytes during the growth stages of *Electrophorus*.

Introduction

Electric fish include multiple classified species, such as electric rays, catfish, and eels. As Charles Darwin described in his work *On the Origin of Species* (Chapter 6: Difficulties on Theory), “The electric organs of fishes offer another case of special difficulty; for it is impossible to conceive by what steps these wondrous organs have been produced” (Darwin, 1859). Darwin's question of how these electric species appeared independently in each taxon is difficult and remains elusive. Here, we address this question from the perspective of cell and molecular biology using electric eels (*Electrophorus*).

The electric eel, an electric fish, was originally described by Carl Linnaeus in 1766 as *Gymnotus electricus* and was later revised as *Electrophorus electricus* by Theodore Gill in 1864 (Jordan, 1963). Recently, they have been reclassified into three distinct species, *E. electricus*, *Electrophorus varii*, and *Electrophorus voltai*, based on both morphological and genetic sequence data (de Santana et al., 2019). Electric eels are known for their ability to generate electric discharges, with a maximum capacity of 860 V for *E. voltai* (de Santana et al., 2019). They possess three types of electric organs (EOs): the main electric organ (mEO), Hunter’s organ, and Sachs’ organ, which are located in the lateral-ventral region of the tail (Williamson, 1775; Hunter, 1775; Sachs, 1877). The mEO is the largest among the three. It appears as early as the juvenile stage (total length [TL], 15 mm) (Schwassmann et al., 2014), but the other two appear at later stages, around a TL of 23 cm (Moller, 1995). The mEO is predicted to play a role in high-voltage discharge for prey capture or defense, whereas the other organs are considered to play a role in low-voltage discharge for sensing and communication (Xu et al., 2021). The cells responsible for electric discharge in an EO are multinucleated syncytia called electrocytes (Luft, 1957). Early studies suggested that electrocytes are derived from muscle lineage precursors (Fritsch, 1883). Recent histological observations of the mEO in juvenile

63 *Electrophorus* suggest that the EO consists of electrocytes budded from a specified cell cluster
64 named the electromatrix, located in the ventral region of the skeletal muscle (Schwassmann et
65 al., 2014). More detailed observations and multifaceted analyses of *Electrophorus* embryos are
66 required to determine the distinct origin and developmental mechanisms of the first electrocytes.
67 However, artificial breeding methods have not yet been established; therefore, obtaining
68 embryos in the laboratory is challenging. As an alternative model, a weakly electric fish,
69 *Brachyhypopomus gauderio*, a species related to *Electrophorus* belonging to the same order
70 (*Gymnotiformes*), was used to observe developmental stages, including EOs, under laboratory
71 conditions (Alshami et al., 2020). In this species, cell clusters consisting of $Pax7^{+}$/$Myosin^{-}$ cells
72 in the ventral region of the myotome were reported as the EO primordium. Based on these
73 studies, the developmental origin of electrocytes in electric species of *Gymnotiformes* is
74 considered to be the ventral cell cluster derived from somite lineage cells rather than from
75 differentiated myocytes. In these studies, electrocyte lineage cells were classified into two
76 populations: mature electrocytes and immature cells located in the ventral cluster. However,
77 suppose one or both stages consist of multiple “substages.” In this case, their clarification is
78 expected to lead to a more detailed description of the differentiation process of electrocyte
79 lineage cells. Moreover, researchers have focused on the developmental origin of electrocytes;
80 however, the source of these cells during growth remains elusive.
81 From another perspective, advances in molecular biology methods have enabled the
82 comparison of gene expression between EOs and other tissues, including skeletal muscle. In
83 EOs, some muscle characteristic genes were downregulated, whereas other genes not
84 expressed in the muscle were upregulated (Gallant et al., 2014; Gallant, 2019). Specifically,
85 genes for ion transporters or channels, such as *atp1a*, *chrna*, *scn4aa*, and *kcnj12*, are
86 upregulated not only in electric eels, but also in other electric fish species (Thompson et al.,

87 2018; LaPotin et al., 2022). Some functional mutations were found in the genes encoding the
88 ion transporters of *Electrophorus* compared to non-electric species. Substitutions in the amino
89 acid sequences of these proteins have been predicted to contribute to high-voltage discharge in
90 electrocytes (Traeger et al., 2017), and this modification is considered crucial for high-voltage
91 electric discharge in *Electrophorus* spp. The molecular genetic characteristics of mature
92 electrocytes are well known; however, how these expressed genes affect the differentiation of
93 electrocytes remains unknown. Here, we report the progenitors of electrocytes based on
94 histological observations and immunohistochemistry. Understanding the spatiotemporal
95 distribution of ion transporter proteins in the EO is essential for understanding electrocyte
96 differentiation.

Results

Morphological observations of electrocytes

Electrophorus has its mEO in the tail region, which is the largest of the three organs responsible for electric discharge. In this study, especially in the histological analysis, the specimens were regarded as too young to observe well-developed Hunter's and Sach's organs; thus, they were excluded from the analysis. The mEO is located ventral to the skeletal muscle and consists of multinucleated syncytia called electrocytes (Figure 1A, 1B). The electrocytes were layered along the dorsal–ventral and anterior–posterior axes (Figure 1B). The series of cells along the anterior–posterior axis increases the membrane potential and generates a high-voltage discharge. Cell morphology along the dorsal–ventral axis is critical for understanding how electrocytes develop in the body; thus, we examined the histological morphology of electrocytes using MT staining (Figure 1C, Figure S1). In the dorsal region of the mEO, we observed the typical structure of mature multinucleated electrocytes placed in a non-cellular compartment with an extracellular space around the cell body, which is important for generating a membrane potential for discharge. In the ventral region, such distinct extracellular spaces were not observed, and square cell bodies without protrusions filled the compartment (Figure 1D, Figure S1, S2). This morphological difference was also confirmed by the observation of toluidine blue-stained ultrathin sections and electron microscopy. Electron microscopy indicated that ventral electrocyte nuclei exhibited various shapes compared with those in the dorsal region. The presence and morphology of the mitochondria and caveolae showed no distinct differences between cells in the dorsal and ventral regions (Figure 1E). Through these experiments, we identified electrocytes with a previously unreported morphology in the ventral region of the mEO.

Ventral terminal cell cluster in EO

The cell morphology of the mEO differed between the dorsal and ventral regions. Thus, a detailed examination of the cell morphology from the ventral to the dorsal terminus of the mEO was performed using HE and MT staining (Figure 2A, Figure S3, S4). A characteristic cell cluster consisting of high-density nuclei was identified at the ventral terminus of the mEO. This cluster was separated from the adjacent muscle layer by collagen fibers. In contrast, a structural border was not observed between the cluster and the dorsal region of the mEO (Figure 2B). The anti-myosin signal, which labels myogenic cells, was not detected in ventral cluster cells (Figure 2C, Figure S5). This indicates that the cluster belonged to the mEO, but not the muscle layer. We then categorized the mEO into seven populations based on cell and tissue morphology (Figure 2D, Figure S6). The terminal cluster consisted of high-density mononuclear cells located in the ventral terminus of the mEO, and segregated cell clusters were observed in the dorsal position of the terminal cluster. Layers consisting of mononuclear cells appeared near the dorsal region. Proliferating cells in these layers and multinucleated electrocytes without extracellular space (immature electrocytes) were observed deep in the dorsal region. Mature electrocytes with extracellular spaces were observed over a broad area of the mEO. Finally, the mature mEO appeared to shrink near the dorsal skeletal muscles (Figure 2E, Figure S7). Thus, the morphology of the cells in the mEO changed drastically along the dorsal–ventral axis.

Gene expression in EO

Tissue fragments from the mEO and skeletal muscles were excised via macroscopic surgery, and total RNA was extracted from each tissue. The RNA samples were subjected to NGS, and the resulting sequence reads were processed to determine gene expression values and visualize differences in gene expression between tissues (Figure 3A, Table S1, S2). Our

145 analysis revealed higher expression levels of typical muscle functional factors, such as genes
146 for actin, creatine kinase, myosin, and troponin, in the muscle compared to the mEO.
147 Conversely, *N-myc downstream-regulated gene-4* (*ndrg4*) was found to be more highly
148 expressed in the mEO (Table S3). The present study focused specifically on the membrane
149 molecules responsible for generating membrane potential through ion transport, such as
150 acetylcholine receptors and sodium/potassium transporters, which exhibit higher expression
151 levels in the mEO than in skeletal muscle (Figure 3B, Table S3). Notably, genes encoding NKA
152 subunits (*atp1a2a* and *atp1b2b*) were highly expressed in the mEO, based on RNA sequencing.
153 Cation transporters are believed to be localized in the anterior part of electrocytes (Figure 3C).
154 In the tail region of *Electrophorus*, the electrocytes align along the anterior-posterior axis of the
155 trunk, which is responsible for generating a high-voltage current due to synchronous activation
156 regulated by motor neurons (Figure 3D).
157
158 *NKA distribution in EO*
159 To evaluate electrocyte function, the presence and distribution of NKA protein in the mEO were
160 detected using immunohistochemistry. The anti-NKA supernatant exhibited specific signals in
161 the mEO and other organs, including the skeletal muscle and central nervous system, in
162 *Electrophorus* (Figure 3E, Figure S8, S9). In the electrocytes, the plasma membrane of the
163 mEO was labeled with the supernatant. The sagittal section indicated the accumulation of NKA
164 protein in the anterior part of the plasma membrane (Figure 3F, Figure S8–S11). Additionally,
165 the signals were lower in the ventral region of the mEO and absent in the ventral terminal
166 cluster, even after longer chromogenic reactions (Figure 3G, 3H, Figure S12, S13). NKA
167 expression was detected in the initial layer stages in the mEO, but the signals did not exhibit
168 membrane localization, which was observed during proliferation. Subsequently, strong

169 membrane NKA signals were observed in immature and mature mEO tissues. An NKA signal
170 was also detected in the shrunken tissue (Figure 3H). These data indicate that NKA is absent in
171 the terminal cluster cells of the mEO but is upregulated and membrane-localized in the dorsal
172 population cells, including mature electrocytes.
173

174 **Discussion**

175 We analyzed the generation of electrocytes in *Electrophorus* using histology and
176 immunohistochemistry. Our analysis indicated that ventral cluster cells are promising electrocyte
177 progenitor candidates in the mEO. We propose that these progenitor cells differentiate into
178 electrocytes and migrate from the ventral to the dorsal region. NKA expression is absent in the
179 ventral cluster, initiating from the monocellular stages and maintaining its expression in
180 developed multicellular electrocytes. This is the first report to provide consecutive observations
181 of EO development, indicating the origin of electrocytes in the post-embryonic stages of
182 *Electrophorus*. Early studies alleged that EOs in electric fish were derived from muscle fibers or
183 muscle lineage cells, based on morphological observations. Histological observations of electric
184 rays and larval mormyrid fish suggest that their electrocytes differentiate from mature muscle
185 fibers (Fox and Richardson, 1978; Srivastava and Szabo, 1972). In *Electrophorus*, electrocytes
186 were considered to differentiate from muscle based on light microscopy observations (Fritsch,
187 1883; Szabo, 1966). These studies concluded that the presumed electrocyte progenitors
188 exhibited striated muscle-like structures. In our study, such muscular structures were not found
189 in the ventral region of the mEO, and the ventral muscle layer was separated from the mEO by
190 collagen fibers. Furthermore, the mEO lacked myosin-positive cells, which are characteristic of
191 muscle tissue. Therefore, our results do not support the hypothesis that the electrocytes of
192 *Electrophorus* are derived from muscle lineage cells.

193 Other groups have claimed that electrocytes do not originate from differentiated muscle
194 lineage cells, but are directly developed from mesodermal cells before cell fate commitment
195 (Keynes 1961). Histological observations have identified cell clusters ventral to the myotome as
196 potential precursors of electrocytes in *Electrophorus* and related species, such as the weakly
197 electric *Brachyhypopomus gauderio* (Schwassmann et al., 2014; Alshami et al., 2020).

198 However, they classified the candidate cluster and the developed EO as independent tissues in
199 different locations, leaving no clear evidence to suggest a relationship between them. They
200 used *Electrophorus* embryos obtained from the field because experimental breeding methods
201 for handling embryos in laboratories had not yet been established. This problem still exists and
202 does not allow the use of embryos in our experiment. Therefore, in the present study, juvenile
203 fish prior to sexual maturation were used.
204 We identified a ventral terminal cell cluster in the mEO and observed continuous changes in
205 cell morphology. Based on these data, we propose that the electrocytes originate as
206 mononuclear progenitor cells in the ventral terminal cluster of the mEO and differentiate into
207 multinucleated syncytia with dorsal migration (Figure 4). Although this study was limited by
208 breeding methodology challenges in obtaining embryos under laboratory conditions and did not
209 focus on embryonic stages, our findings on the source and differentiation of electrocytes during
210 growth are crucial for understanding the molecular mechanisms underlying EO formation in
211 *Electrophorus*.
212 We focused on sodium potassium adenosine triphosphatase (Na^+/K^+-ATPase, NKA) as a
213 functional molecule involved in generating membrane potential in electrocytes. We observed
214 that the transcripts per million values for the NKA subunits in the mEO were over 100-fold
215 higher than those in the skeletal muscle. A previous study identified novel phosphorylation sites
216 in the NKA protein of electric eels that were predicted to contribute to the high-voltage discharge
217 of EOs (Traeger et al., 2017). NKA is ubiquitously distributed in animal tissues and plays an
218 important role in generating membrane potential for cellular functions beyond those of
219 electrocytes (Suhail, 2010). NKA is a popular sodium pump distributed not only in EOs but also
220 in various types of cells; thus, anti-NKA signals were detected not only in the mEO but also in
221 the skeletal muscle, kidney, brain, and other organs of *Electrophorus*. Notably, the ventral region

222 of the mEO lacked anti-NKA signals, suggesting that ventral cluster cells are immature and
223 unable to generate membrane potentials via the NKA ion pump. Cells in the ventral terminal
224 cluster exhibit characteristic morphologies, such as small size, minimal cytoplasm, and round
225 shape, which are typical characteristics of quiescent stem cells, including hematopoietic stem
226 cells (HSCs) and muscle satellite cells (MuSCs) (de Morree & Rando, 2023; Pinho & Frenette,
227 2019; Siegel et al., 2011). Therefore, we propose that the ventral terminal cluster includes stem
228 cells that differentiate into electrocytes. Furthermore, single-cell RNA sequencing or cell
229 characteristic evaluation using stem cell markers contributes to a deeper understanding of the
230 maintenance of terminal cluster cells and their differentiation into electrocytes. Methodological
231 investigations using *Electrophorus* should be improved in future research.
232 Our finding that multinucleated cells in the dorsal region of the mEO more closely resemble the
233 typical morphology of functional electrocytes than those in the ventral region supports the
234 conventional theory that the ventral region includes electrocyte progenitors (Gotter et al., 1998).
235 Electrocytes in the dorsal terminus of the mEO shrank, and the tissue structure appeared to be
236 disrupted. Therefore, we propose that the EO develops from stem cells in the ventral region,
237 progresses to maturity with dorsal migration, and eventually regresses in the dorsal terminal.
238 This 'Ventral-to-Dorsal' model does not conflict with previous reports (Szabo, 1966;
239 Schwassmann et al., 2014). Our study enhances the understanding of the developmental
240 process of EOs in *Electrophorus*. Further analyses using cutting-edge technologies, including
241 NGS, are required to understand the molecular mechanisms by which EOs are generated in
242 *Electrophorus*. A recent study proposed that changes in sodium channel expression are
243 important for the evolutionary acquisition of EOs in weakly electric species (LaPotin et al.,
244 2022). Darwin's question arose from the independent acquisition of EOs in several fish
245 lineages. The present study provides detailed information on the origin and developmental

process of EOs in the electric eel *Electrophorus*. Future application of our methods to other electric fish may ultimately lead to a solution to Darwin's question.

Methods

Animal experiments

This study was approved by the Ethics Review Board for Animal Experiments at Nagoya University (approval number: A240105-002). All experiments involving live animals were conducted in strict accordance with institutional guidelines to ensure humane treatment. Electric eels used in this study were purchased from Meito Suien Co., Ltd. (Nagakute, Japan). The specimens used for histology were too young (TL: 10–15 cm) to determine their distinct species and sex; thus, we treated them as *Electrophorus sp*. (*Electrophorus*) in this study. The specimen used for sequencing analysis was a female with a developed ovary and was presumed to be *E. electricus* based on genome information.

Histology and histochemistry

The electric eels were euthanized using a rapid cooling shock to ensure that they were unresponsive to gill movements and external stimuli (Wilson et al., 2009). Tail region cross-sections (5 mm thick) were dissected and fixed in 4% paraformaldehyde solution for 24 h at room temperature for histological observations. Fixed samples were then dehydrated in a graded ethanol series, cleared in xylene, embedded in paraplast, and sectioned at 4 μm thickness using a Leica microtome (Leica, Germany) (Kongthong et al., 2023; Presnell and Schreibman, 2013; Suvarna et al., 2013). Three consecutive sections were stained with Harris' hematoxylin and eosin (HE) to observe body organization and tissue structure. Masson's trichrome (MT) staining was used to assess muscular structure and collagen fibers. Tissue samples were examined, photographed using an Olympus BX53 microscope, and imaged using a DP25 digital camera (Olympus, Shinjuku, Japan) or a BZ-X800 microscope (Keyence, Osaka, Japan).

Electron microscopy

The tail region of *Electrophorus* was sliced into 5 mm transverse sections and fixed in 2.5% glutaraldehyde, followed by washing with PBS. The fixed specimens were treated with 1% osmium tetroxide in PBS for 60 min and dehydrated in a graded ethanol series (50%, 70%, 80%, 90%, 95%, 99.5%, and 100%). Samples were treated with propylene oxide (KISHIDA CHEMICAL, Osaka, Japan) and embedded in epoxy resin (Nissin EM Quetol-812). The blocks were polymerized at 60°C for 48 h. Sections of 1 μm thickness were stained with toluidine blue and observed using a Nikon ECLIPSE LV100ND with a DP74 digital camera (Olympus) to determine the region of interest. Sections of 100 nm thickness were cut using a Leica ultramicrotome and stained with UranyLess (Micro to Nano) and 3% lead citrate (Micro to Nano). Backscattered electron images were obtained using an SU9000 field-emission scanning electron microscope (Hitachi, Tokyo, Japan) at 1 kV.

RNA sequencing

Total RNA was extracted from the mEO and skeletal muscle of an adult female electric eel using an RNeasy Plus Mini kit (QIAGEN). Next-generation sequencing (NGS) was performed by Macrogen Japan Corp. (Tokyo, Japan) using a NovaSeq6000 platform (Illumina, Inc., San Diego, CA, USA). Approximately 40 million 100 bp paired-end reads were obtained for each sample. NGS data were deposited in the DNA Data Bank of Japan (DDBJ; ID: PRJDB17973).

Transcriptomic analysis

The calculation of differentially expressed genes was performed using the National Institute of Genetics' supercomputer at the Research Organization of Information and Systems. The

296 adaptor and noise sequences were removed using the fastp program version 0.23.2
297 (https://github.com/OpenGene/fastp) (Chen et al., 2018). The cleaned reads were mapped to
298 the genome of *Electrophorus electricus* (GCA_003665695.2,
299 https://asia.ensembl.org/*Electrophorus*_electricus/Info/Index/) using the HISAT2 program
300 version 2.2.1 (https://daehwankimlab.github.io/hisat2/) (Kim et al., 2019). The number of
301 mapped reads was calculated using the featureCounts program in the subread package version
302 2.0.6 (https://subread.sourceforge.net/) (Liao et al., 2013, 2014). Further calculations were
303 performed using the R software on a personal computer. Differentially expressed genes were
304 identified using the edgeR package version 3.42.4
305 (https://bioconductor.org/packages/release/bioc/html/edgeR.html) with the following thresholds:
306 false discovery rate < 0.05, and fold change > 2.00 (Robinson et al., 2010). A volcano plot was
307 generated using the enhanced volcano package version 1.20.0
308 (https://github.com/kevinblighe/EnhancedVolcano).
309
310 *Immunohistochemistry*
311 Consecutive sections from the histological protocol were prepared on slides coated with
312 glycerol-albumin (Mayer's fixative). The slides were deparaffinized in xylene, hydrated through a
313 decreasing ethanol series, washed in tap water, and treated with 0.5% Triton X-100/PBS for 30
314 min and 0.3% H_2O_2 for 10 min to inactivate endogenous peroxidase activity. The sections were
315 blocked with Blocking One solution for 2 h at room temperature (03953-95, Nacalai Tesque,
316 Kyoto, Japan). The sections were incubated overnight at 4°C with either anti-NKA α1 (a5-s,
317 DSHB, IA, USA, 1:5 in Blocking-One solution) or myosin heavy chain (F59-s, DSHB, 1:5 in
318 Blocking-One solution) hybridoma supernatants. This was followed by incubation with Horse
319 Anti-Mouse IgG Antibody (H+L) Peroxidase (PI-2000, Vector Laboratories, Inc., Burlingame,

320 CA, USA, 1:500 dilution in 0.1% Tween-20/PBS) for 2 h at 4°C. Staining was performed by
321 incubation with 3,3'-diaminobenzidine tetrahydrochloride (SK-4105, Vector Laboratories, Inc.)
322 for 5 min at room temperature. Finally, the slides were dehydrated and mounted using
323 Permount (SP15-100, Thermo Fisher Scientific). A control section without primary antibody was
324 prepared to ensure the specificity of staining. Sodium-potassium adenosine triphosphatase
325 (Na^+/K^+-ATPase [NKA]) localization was examined and photographed using the same method
326 used for histological observations.
327

Acknowledgments

Computations were partially performed on the supercomputer of the National Institute of Genetics (NIG) at the Research Organization of Information and Systems (ROIS). Yutaka Hattori arranged complimentary rentals of the digital microscope. Akihiko Koga and Akira Kanamori provided us with helpful comments. We are grateful for the constructive discussions with members of Unique-Kai, an annual meeting for biologists investigating non-conventional experimental animals in Japan.

Competing interests

The authors declare no competing interest.

Funding

We acknowledge the fellowship granted to S.S. by the Matsumae International Foundation (Grant Number: MIF-23G04). This work was supported by the Japan Science and Technology Agency (JST), the Japan Society for the Promotion of Science KAKENHI (Grant Number: 21H04637 to M.K.), and the "Advanced Research Infrastructure for Materials and Nanotechnology in Japan (ARIM)" program of the Ministry of Education, Culture, Sports, Science, and Technology (MEXT) (Grant Number: JPMXP1223NU0016 to A.I.).

References

1. Alshami, I. J. J., Ono, Y., Correia, A., Hacker, C., Lange, A., Scholpp, S., Kawasaki, M., Ingham, P. W., & Kudoh, T. (2020). Development of the electric organ in embryos and larvae of the knifefish, Brachyhypopomus gauderio. Developmental biology, 466(1-2), 99–108. https://doi.org/10.1016/j.ydbio.2020.06.010
2. Chen S, Zhou Y, Chen Y, Gu J. fastp: an ultra-fast all-in-one FASTQ preprocessor. Bioinformatics. 2018;34(17):i884-i890. doi:10.1093/bioinformatics/bty560
3. Darwin, C. & Kebler, L. (1859) On the origin of species by means of natural selection, or, The preservation of favoured races in the struggle for life. London: J.
4. de Morree, A., & Rando, T. A. (2023). Regulation of adult stem cell quiescence and its functions in the maintenance of tissue integrity. Nature reviews. Molecular cell biology, 24(5), 334–354. https://doi.org/10.1038/s41580-022-00568-6
5. de Santana, C. D., Crampton, W. G. R., Dillman, C. B., Frederico, R. G., Sabaj, M. H., Covain, R., Ready, J., Zuanon, J., de Oliveira, R. R., Mendes-Júnior, R. N., Bastos, D. A., Teixeira, T. F., Mol, J., Ohara, W., Castro, N. C. E., Peixoto, L. A., Nagamachi, C., Sousa, L., Montag, L. F. A., Ribeiro, F., Waddell, J. C., Piorsky, N. M., Vari, R. P., Wosiacki, W. B. (2019). Unexpected species diversity in electric eels with a description of the strongest living bioelectricity generator. Nature communications, 10(1), 4000. https://doi.org/10.1038/s41467-019-11690-z
6. Fox, G. Q., & Richardson, G. P. (1978). The developmental morphology of Torpedo marmorata: electric organ--myogenic phase. The Journal of comparative neurology, 179(3), 677–697. https://doi.org/10.1002/cne.901790313
7. Fritsch G (1883) Die elektrischen Fische im Lichte der Deszendenzlehre. In: Virchow R, von Holtzendorff FR (eds) Sammlung gemeinverständlicher wissenschaftlicher Vorträge,

vol 835–898. Habel, Berlin

8. Gallant, J. R., Traeger, L. L., Volkening, J. D., Moffett, H., Chen, P. H., Novina, C. D., Phillips, G. N., Jr, Anand, R., Wells, G. B., Pinch, M., Güth, R., Unguez, G. A., Albert, J. S., Zakon, H. H., Samanta, M. P., & Sussman, M. R. (2014). Nonhuman genetics. Genomic basis for the convergent evolution of electric organs. Science (New York, N.Y.), 344(6191), 1522–1525. https://doi.org/10.1126/science.1254432
9. Gallant, J.R. (2019). The Evolution and Development of Electric Organs. In: Carlson, B., Sisneros, J., Popper, A., Fay, R. (eds) Electroreception: Fundamental Insights from Comparative Approaches. Springer Handbook of Auditory Research, vol 70. Springer, Cham. https://doi.org/10.1007/978-3-030-29105-1_4
10. Gotter, A. L., Kaetzel, M. A., & Dedman, J. R. (1998). *Electrophorus* electricus as a model system for the study of membrane excitability. Comparative biochemistry and physiology. Part A, Molecular & integrative physiology, 119(1), 225–241. https://doi.org/10.1016/s1095-6433(97)00414-5
11. Hunter, J. (1775). "An account of the Gymnotus electricus". Philosophical Transactions of the Royal Society of London (65): 395–407.
12. Jordan DS. 1963. The genera of fishes and a classification of fishes. Stanford: Stanford University Press, 330.
13. Keynes RD (1961) The development of the electric organ in *Electrophorus* electricus L. In: Chagas C, Paes de Carvalho A (eds) Bioelectrogenesis. Elsevier, Amsterdam, pp 14–19
14. Kim, D., Paggi, J. M., Park, C., Bennett, C., & Salzberg, S. L. (2019). Graph-based genome alignment and genotyping with HISAT2 and HISAT-genotype. Nature biotechnology, 37(8), 907–915. https://doi.org/10.1038/s41587-019-0201-4
15. Kongthong, K., Charoenphon, N., Thaochan, N., Boonyoung, P., Iida, A., Jeamah, A.,

Imsonpang, S, Wongkamhaeng,K., Kongtheng, P. & Senarat, S. (2023). A histological method for marine invertebrates. Vertinary Intergrative Science 21:251-163.

16. LaPotin, S., Swartz, M. E., Luecke, D. M., Constantinou, S. J., Gallant, J. R., Eberhart, J. K., & Zakon, H. H. (2022). Divergent cis-regulatory evolution underlies the convergent loss of sodium channel expression in electric fish. Science advances, 8(22), eabm2970. https://doi.org/10.1126/sciadv.abm2970
17. Liao, Y., Smyth, G. K., & Shi, W. (2013). The Subread aligner: fast, accurate and scalable read mapping by seed-and-vote. Nucleic acids research, 41(10), e108. https://doi.org/10.1093/nar/gkt214
18. Liao, Y., Smyth, G. K., & Shi, W. (2014). featureCounts: an efficient general purpose program for assigning sequence reads to genomic features. Bioinformatics (Oxford, England), 30(7), 923–930. https://doi.org/10.1093/bioinformatics/btt656
19. Luft, J. H. (1957). The histology and cytology of the electric organs of electric eel (*Electrophorus electricus L.*). Journal of Morphology, 100 (1), 113-139.
20. Moller, P. (1995) Electric fishes: history and behavior. Chapman & Hall, London
21. Pinho, S., & Frenette, P. S. (2019). Haematopoietic stem cell activity and interactions with the niche. Nature reviews. Molecular cell biology, 20(5), 303–320. https://doi.org/10.1038/s41580-019-0103-9
22. Presnell, J.K., & Schreibman, M. P. (1997). Humason's animal tissue techniques, 5th ed. US, Johns Hopkins University Press.
23. Robinson, M. D., McCarthy, D. J., & Smyth, G. K. (2010). edgeR: a Bioconductor package for differential expression analysis of digital gene expression data. Bioinformatics (Oxford, England), 26(1), 139–140. https://doi.org/10.1093/bioinformatics/btp616
24. Sachs, C. (1877). Beobachtungen und versuche am südamerikanischen zitteraale

(*Gymnotus electricus*). Archives of Anatomy and Physiology, 66–95.

25. Schwassmann, H. O., Assunção, M. I., & Kirschbaum, F. (2014). Ontogeny of the electric organs in the electric eel, *Electrophorus* electricus: physiological, histological, and fine structural investigations. Brain, behavior and evolution, 84(4), 288–302. https://doi.org/10.1159/000367884
26. Siegel, A. L., Kuhlmann, P. K., & Cornelison, D. D. (2011). Muscle satellite cell proliferation and association: new insights from myofiber time-lapse imaging. Skeletal muscle, 1(1), 7. https://doi.org/10.1186/2044-5040-1-7
27. Srivastava, C. B., & Szabo, T. (1972). Development of electric organs of Gymnarchus niloticus (fam. Gymnarchidae). I. Origin and histogenesis of electroplates. Journal of morphology, 138(3), 375–385. https://doi.org/10.1002/jmor.1051380305
28. Suhail M. (2010). Na, K-ATPase: Ubiquitous Multifunctional Transmembrane Protein and its Relevance to Various Pathophysiological Conditions. Journal of clinical medicine research, 2(1), 1–17. https://doi.org/10.4021/jocmr2010.02.263w
29. Suvarna, K.S., Layton, C., Bancroft, J.D. (2013). Bancroft's theory and practice of histological techniques. 7th ed. Canada, Elsevier.
30. Szabo T. (1966). The origin of electric organs of *Electrophorus* electricus. The Anatomical record, 155(1), 103–110. https://doi.org/10.1002/ar.1091550112
31. Thompson, A., Infield, D. T., Smith, A. R., Smith, G. T., Ahern, C. A., & Zakon, H. H. (2018). Rapid evolution of a voltage-gated sodium channel gene in a lineage of electric fish leads to a persistent sodium current. PLoS biology, 16(3), e2004892. https://doi.org/10.1371/journal.pbio.2004892
32. Traeger, L. L., Sabat, G., Barrett-Wilt, G. A., Wells, G. B., & Sussman, M. R. (2017). A tail of two voltages: Proteomic comparison of the three electric organs of the electric eel. Science

advances, 3(7), e1700523. https://doi.org/10.1126/sciadv.1700523

33. Williamson, H. (1775). "Experiments and observations on the Gymnotus electricus, or electric eel". Philosophical Transactions of the Royal Society of London (65): 94–101.

34. Wilson, J.M., Bunte, R.M., & Carty, A.J. (2009). Evaluation of rapid cooling and tricaine methanesulfonate (MS 222) as methods of euthanasia in zebrafish (*Danio rerio*). Journal of the American Association for Laboratory Animal Science (48): 785–789.

35. Xu, J., Cui, X., & Zhang, H. (2021). The third form electric organ discharge of electric eels. Scientific reports, 11(1), 6193. https://doi.org/10.1038/s41598-021-85715-3

452 **Figures**

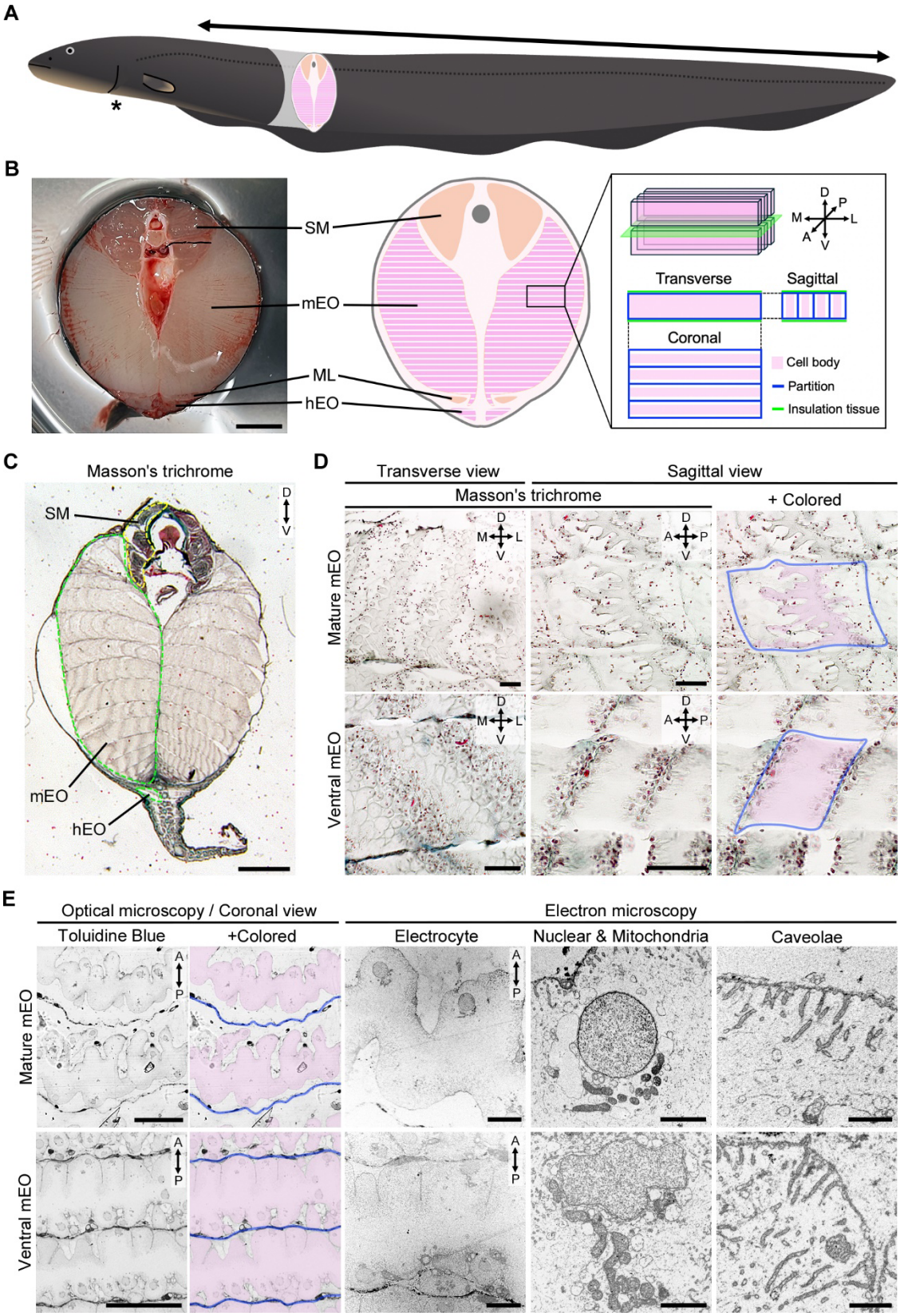

453

454 **Figure 1. Morphological differences of multinucleated electrocytes**

455 **A**. Illustration of the whole body of *Electrophorus*. The double-headed arrow corresponds to the
456 tail region of the body. The asterisk indicates the anus. **B**. A photograph and illustration of the
457 transverse section of the tail region of *Electrophorus*. The medial–lateral lines in the mEO
458 indicate the outer edge of the multinucleated electrocytes. The plate-shaped electrocytes are
459 stacked along the anterior–posterior and dorsal–ventral axes. SM, skeletal muscle. mEO, main
460 electric organ. Scale bar, 1 cm. **C**. A whole transverse section of the tail region, including the
461 electric organ. Scale bar, 1 mm. **D**. Cell morphologies of the electrocytes in the dorsal and
462 ventral regions of the mEO. The blue lines indicate the outer edges of the electric unit. The cell
463 bodies of electrocytes (colored magenta) are within the unit. Scale bars, 50 μm. **E**. Ultrathin
464 sections (100 nm) of the electrocytes observed by optical or electron microscopy. The blue lines
465 indicate the outer edges of the electric unit. The cell bodies of electrocytes (colored magenta)
466 are within the unit. Scale bars, 50 μm (toluidine blue), 10 μm (electrocyte), 2 μm (nucleus &
467 mitochondria), 1 μm (caveolae). A, anterior; D, dorsal; M, medial; L, lateral; P, posterior; V,
468 ventral; hEO, Hunter's electric organ; mEO, main electric organ; SM, skeletal muscle.

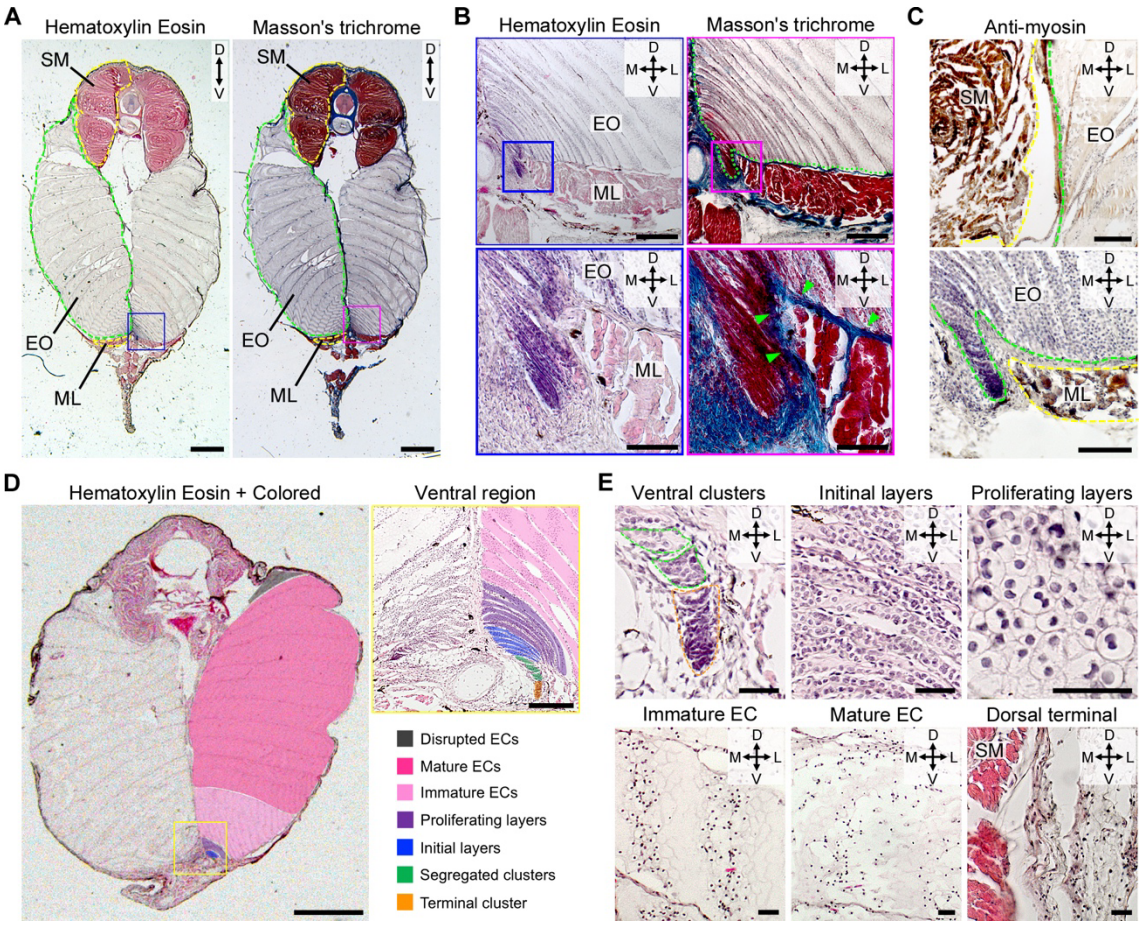

Figure 2. Morphological differences of cells along the dorsal–ventral axis

A. A whole transverse section of the tail region, including the electric organ. The green dotted line indicates the outer edge of the mEO. The yellow dotted lines indicate the outer edge of the muscular tissues. Scale bar, 1 mm. **B**. The ventral region of the mEO and the enlarged images of the ventral terminal cluster. The green dotted line indicates the outer edge of the mEO. The green arrowheads indicate the collagen fibers stained by Aniline Blue. Scale bars, 200 μm (low magnification), 50 μm (enlarged). **C**. Immunohistochemistry against myosin heavy chain in the dorsal and ventral positions. The muscular tissues show positive signals, but not in the mEO tissues. Scale bars, 100 μm (dorsal), 50 μm (ventral).

D. A whole transverse section colored roughly by cell morphology. Scale bars, 1 mm (whole section), 100 μm (enlarged). **E**. Enlarged images of each cell type in the mEO. The orange

481 dotted line indicates the terminal ventral cluster. The green dotted lines indicate the segregated

482 cell clusters. Scale bar, 20 μm. D, dorsal; M, medial; L, lateral; V, ventral; mEO, main electric

483 organ; ML, muscle layer; SM, skeletal muscle.

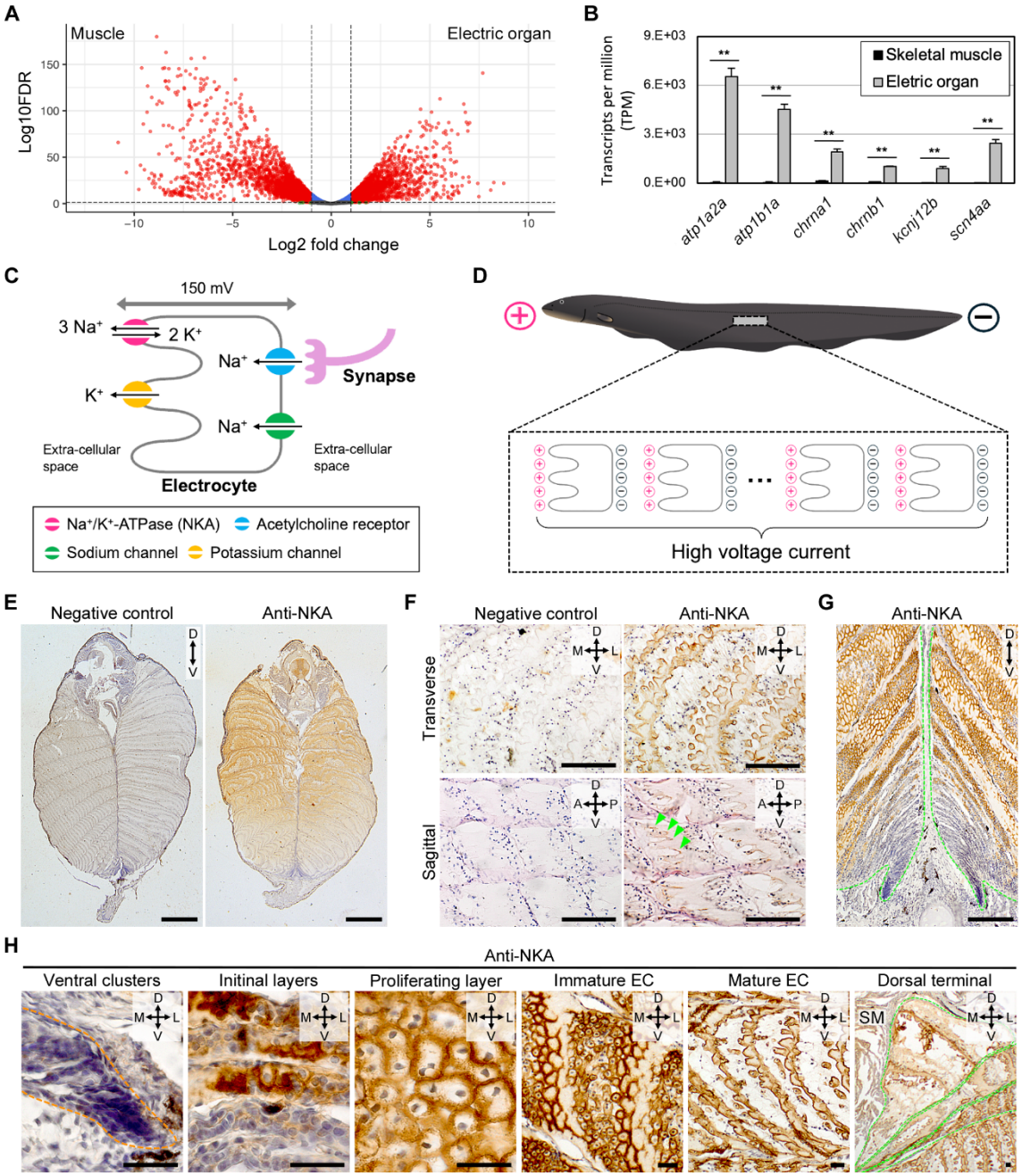

Figure 3. Presence and distribution of Na+/K+-ATPase in electric organ

A. Volcano map showing differentially expressed genes between skeletal muscle and mEO. Source data deposited in the DDBJ (ID: PRJDB17973). **B**. Comparison of gene expression values (TPM) for Na^+/K^+-ATPase (*atp1a2a*, *atp1b1a*), acetylcholine receptor (*chrna1*, *chrnb1*), potassium channel (*kcnj12b*), and sodium channel (*scn4aa*) between skeletal muscle and mEO.

490 **C**. Schematic model illustrating the generation of membrane potential in an electrocyte, with ion
491 transporters localized anteriorly or posteriorly on the cell surface, generating approximately 150
492 mV current due to synaptic input. **D**. Electrocytes arranged along the anterior–posterior axis,
493 enhancing membrane potential leading to high-voltage discharge. **E**. Immunohistochemistry
494 against NKA in transverse section. Scale bars, 1 mm. **F**. Enlarged images of anti-NKA
495 immunohistochemistry in dorsal mEO in transverse and sagittal sections. Green arrowheads
496 indicate anti-NKA signals on the anterior cell surface. Scale bars, 100 μm (transverse), 50 μm
497 (sagittal). **G**. Ventral half of mEO in anti-NKA immunohistochemistry. Weaker anti-NKA signals
498 observed in ventral terminal compared to dorsal regions. Scale bar, 100 μm. **H**. Enlarged
499 images of anti-NKA immunohistochemistry in each cell type in the mEO. Orange dotted line
500 indicates terminal ventral cluster. Green dotted lines indicate three layers from dorsal terminal of
501 the mEO. Scale bar, 20 μm. A, anterior; D, dorsal; M, medial; L, lateral; P, posterior; V, ventral;
502 SM, skeletal muscle.

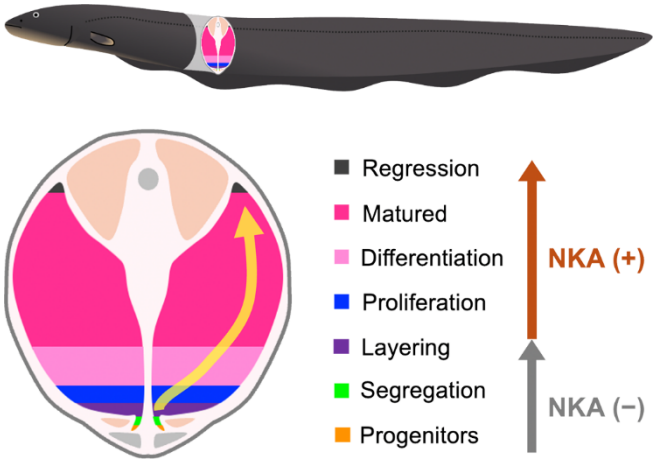

Figure 4. Model of main electric organ development

This illustration indicates the development of the main electric organ in the adult electric eel. Progenitor cells located in the ventral terminus of the main electric organ segregate and migrate dorsally, forming a layered structure. The NKA ion pump begins to be expressed at this stage. The cells in this layer proliferate and fuse into multinucleated syncytia. The syncytia differentiate into mature electrocytes and contribute to the generation of high-voltage discharges via ion transporters, including NKA. Electrocytes may regress to the dorsal terminus of the main electric organ.